A&A 588, A32 (2016)
DOI: 10.1051/0004-6361/201527973

Astronomy & Astrophysics

Atmospheric conditions at Cerro Armazones derived from astronomical data⋆,⋆⋆

Maša Lakićević[1], Stefan Kimeswenger[1,2], Stefan Noll[2], Wolfgang Kausch[3,2], Stefanie Unterguggenberger[2], and Florian Kerber[4]

[1] Instituto de Astronomía, Universidad Católica del Norte, Av. Angamos, 0610 Antofagasta, Chile
e-mail: [mlakicevic;skimeswenger]@ucn.cl
[2] Institute for Astro- and Particle Physics, University of Innsbruck, Technikerstr. 258, 6020 Innsbruck, Austria
[3] University of Vienna, Department of Astrophysics, Türkenschanzstr. 17 (Sternwarte), 1170 Vienna, Austria
[4] European Southern Observatory, Karl-Schwarzschild-Str. 2, 85748 Garching bei München, Germany

Received 15 December 2015 / Accepted 30 January 2016

ABSTRACT

Aims. We studied the precipitable water vapour (PWV) content near Cerro Armazones and discuss the potential use of our technique of modelling the telluric absorbtion lines for the investigation of other molecular layers. The site is designated for the European Extremely Large Telescope (E-ELT) and the nearby planned site for the Čerenkov Telescope Array (CTA).
Methods. Spectroscopic data from the Bochum Echelle Spectroscopic Observer (BESO) instrument were investigated by using a line-by-line radiative transfer model (LBLRTM) for the Earth's atmosphere with the telluric absorption correction tool `molecfit`. All observations from the archive in the period from December 2008 to the end of 2014 were investigated. The dataset completely covers the El Niño event registered in the period 2009–2010. Models of the 3D Global Data Assimilation System (GDAS) were used for further comparison. Moreover, we present a direct comparison for those days for which data from a similar study with VLT/X-Shooter and microwave radiometer LHATPRO at Cerro Paranal are available.
Results. This analysis shows that the site has systematically lower PWV values, even after accounting for the decrease in PWV expected from the higher altitude of the site with respect to Cerro Paranal, using the average atmosphere found with radiosondes. We found that GDAS data are not a suitable basis for predicting local atmospheric conditions – they usually systematically overestimate the PWV values. The large sample furthermore enabled us to characterize the site with respect to symmetry across the sky and variation with the years and within the seasons. This technique of studying the atmospheric conditions is shown to be a promising step into a possible monitoring equipment for the CTA.

Key words. site testing – instrumentation: spectrographs – techniques: spectroscopic – methods: observational – atmospheric effects – methods: numerical

1. Introduction

Site selection and characteristics are often based on long-term campaigns with mainly ground-based facilities (Mahoney et al. 1998; Schöck et al. 2009; Vernin et al. 2011; Vázquez Ramió et al. 2012), calibrated by a few in situ verifications. These campaigns measure meteorological parameters such as temperature, humidity, wind speed and direction, ambient pressure near the surface, and seeing conditions. All these facilities are calibrated on other sites with already existing enhanced astronomical facilities, assuming similar ratios of ground layer to general properties of the atmosphere (Varela et al. 2014). In the context of site testing for the Giant *Magellan* Telescope (GMT), the Thirty Meter Telescope (TMT), and the European Extremely Large Telescope (E-ELT), the determination of atmospheric precipitable water vapour (PWV) from optical absorption spectroscopy has been established as a standard approach (Querel et al. 2011).

Another innovation was the use of microwave radiometers deployed at several potential sites (Otárola et al. 2010; Kerber et al. 2010, 2012). Multi-wavelength radiometers, such as the Low Humidity And Temperature PROfiling microwave radiometer (LHATPRO[1]) used at ESO, are capable of providing profiles of the distribution of water vapour in the atmosphere. The commonly accepted verification for such measurements with balloon-borne radiosondes was reported by Kerber et al. (2012). The results agree well with those of the radiosondes. Hence, further measurements can be directly verified with radiometer data (at least in desert zones like Cerro Paranal). The LHATPRO is a radiometer measuring at a frequency of 183 GHz and is hence especially well suited for operations in extremely dry conditions such as the Atacama desert (Rose et al. 2005). It has been deployed on Paranal as a tool to support VLT science operations and has been operational since 2012 (Kerber et al. 2012). Its measurements have been instrumental in documenting episodes of extremely low PWV (well below 0.5 mm, Kerber et al. 2014).

To develop local atmospheric models that are based on the astronomical data, all the above mentioned facilities are combined. The global models, from worldwide weather and

⋆ Based on archival observations collected at the European Organisation for Astronomical Research in the Southern Hemisphere, Chile and of the Cerro Armazones Observatory facilities of the Ruhr Universität Bochum.

⋆⋆ Full Table 1 is only available at the CDS via anonymous ftp to `cdsarc.u-strasbg.fr` (`130.79.128.5`) or via `http://cdsarc.u-strasbg.fr/viz-bin/qcat?J/A+A/588/A32`

[1] Radiometer Physics GmbH, `http://www.radiometer-physics.de/`

climate data calculations (e.g. 3D Global Data Assimilation System (GDAS)[2] models) are used as starting points for the fitting procedures of the astronomical data, which scale the modelled molecular abundance profiles (Smette et al. 2015). This allows determining individual absorption of molecules like ozone, which is required for instance for the data reduction of experiments like the Čerenkov Telescope Array (CTA). Furthermore, this allows characterizing a site for its homogeneity and asymmetries in the water vapour content caused by dominating local ground layer air streams, for example, which is important for observations with the E-ELT in the infrared spectral bands. An even more sophisticated solution was presented recently, using local refinement calculations around the site (Lascaux et al. 2015; Chacón et al. 2011; Marín et al. 2015). The numerical weather prediction models, in particular those running at high horizontal and vertical resolution, require extensive computing time, and they are not always readily available to support the operations and astronomical observations program.

Noll et al. (2012) designed a detailed sky model of Cerro Paranal for ESO. In a follow-up project, the software `molecfit` was designed for the Earth's lower atmosphere in local thermodynamic equilibrium (Smette et al. 2015). `Molecfit` is applied to the astronomical spectroscopic data to determine the atmospheric conditions at the time of the observation. It uses the radiative transfer code LNFL/LBLRTM[3] (Clough et al. 2005). The latter incorporates the spectral line parameter database `aer_v_3.2`, based on HITRAN[4] (Rothman et al. 2009). Furthermore, `molecfit` uses a model of the altitude-dependent chemical composition of the atmosphere obtained from a combination of the ESO MeteoMonitor[5], a standard atmosphere[6], and the GDAS model provided by the National Oceanic and Atmospheric Administration (NOAA; time-dependent profiles of the temperature, pressure, and humidity). The code calculates the amount of atmospheric molecules by scaling the atmospheric profiles iteratively with the radiative transfer code LNFL/LBLRTM (Clough et al. 2005). By fitting the telluric absorption features of the theoretical spectrum to the observed one, a final best-fit profile is achieved, which is assumed to be representative of the state of the atmosphere at the time of observation. This finally allows determining the column densities of the incorporated molecular species.

Kausch et al. (2014) reported the verification of the results against the same LHATPRO that was used for a comparison with the balloon experiments in Kerber et al. (2012). We found that the median difference between the PWV from `molecfit` and from LHATPRO was 0.12 mm with $\sigma = 0.35$ mm. The program package is designed for robustness against inaccurate initial values. Thus, it is suited for an automatic batch mode capability, as is included for pipelines. Moreover, it is able to run "on the fly" in monitoring during operations, as has been proposed in Skidmore & Travouillon (2015) for TMT on Mauna Kea, for example. Kimeswenger et al. (2015) thus proposed a small telescope with a fiber optic spectrograph for a site of the CTA operations.

We here present, to our knowledge, for the first time a spatially resolved study for the designated site of the E-ELT, which is also nearby the recently proposed location for the CTA. Moreover, our study covers six years and includes El Niño (a quasi periodic change of the South Pacific climate; Ludescher et al. 2013). Neither were included in the previous site study for the TMT (Otárola et al. 2010), covering only about 200 days of radiometer data and containing no information on the spatial distribution. We were able to characterize the water vapour distribution and discuss the potential of the technique used here for further extensions towards the CTA.

2. Data

The astronomical observations were made with BESO, a fibre-fed high-resolution spectrograph at the Observatorio Cerro Armazones (OCA), located 22 km from Cerro Paranal in the Atacama desert in Chile (Steiner et al. 2006, 2008; Hodapp et al. 2010; Fuhrmann et al. 2011). The location is 1.45 km SW (direction 221°) from the main summit of Cerro Armazones and is often called Cerro Murphy, at an altitude of 2817 m, about 200 m below the E-ELT site. The proposed CTA site is 15.4 km SW (direction 227°) from our observatory. The instrument covers wavelengths from 370 to 840 nm, with a mean instrumental spectral resolution of about $R \sim 50\,000$. The products of a dedicated data reduction pipeline (Fuhrmann et al. 2011) were used for this study. These fully reduced data sets were provided by the Bochum team. The spectra from 2008 to 2010 were taken at the 1.5 m hexapod telescope. Since 2011, spectra were taken at the 0.83 m IRIS telescope. The observations typically cover 16 days on average per month. The observation days were selected not only by means of best weather conditions, but mainly by the science cases of the observers, such as deriving orbits and radial velocities of binary stars. These data are without spectrophotometric calibration. The data selection was obtained by an automated statistical quality check during the analysis itself, which is described in detail in the following section. There are some differences and inhomogeneities of the data obtained with the two telescopes, such as existing header keywords and the length of the obtained spectrum. For a small fraction of less than 100 files a unique reconstruction of observing time, airmass, etc. was not possible, and thus they were rejected.

In total, data from 996 nights exist from the period from 2008 to 2014. The observed stars are distributed across the whole sky, with a slight concentration towards the Galactic plane, covering the sky well up to a zenith angle of $z \approx 60°$. Only a handful of stars exceed this limit. The sample distribution is shown in Fig. 1.

The PWV data for the Cerro Paranal sample was taken from Kausch et al. (2015). This data set contains several months of the LHATPRO microwave radiometry data campaign that covered various seasons in 2012 and about three years of data taken in the infrared by the VLT instrument X-Shooter.

3. Methods and analysis

3.1. Analysis of the BESO sample with `molecfit`

An example of a BESO spectrum is shown in Fig. 2. The spectra contain telluric absorption bands of the O_3, O_2, and H_2O molecules (Smette et al. 2015). For each spectra we separately fitted H_2O in the two narrow ranges that are indicated in the figure. `Molecfit` calculates the PWV values normalized to zenith. The fits for the two ranges were obtained independently to check for the quality of the pipeline-reduced data. As these ranges originate from the same populations of the roto-vibrational H_2O (211←000) band and thus from the same volume along the line of sight, they are expected to give

[2] http://www.ready.noaa.gov/gdas1.php
[3] http://rtweb.aer.com/lblrtm_frame.html
[4] http://www.cfa.harvard.edu/hitran/
[5] http://archive.eso.org/asm/ambient-server
[6] http://www.atm.ox.ac.uk/RFM/atm/

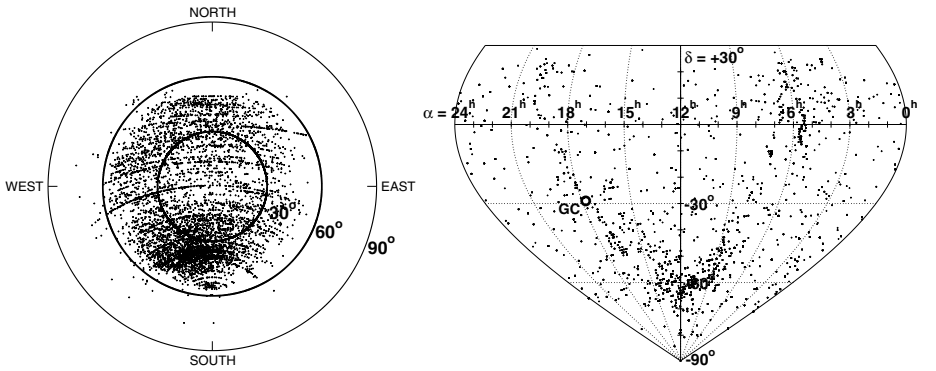

Fig. 1. *Left panel*: distribution of the sample sources on the sky. The vast majority of sources was taken at zenith distances below 60° (≡airmass <2.0). *Right panel*: source distribution on the celestial sphere in Eckert-Greifendorff projection. The sources are fairly homogeneously distributed with only a slight enhancement towards the Galactic plane. The Galactic centre is marked with a circle.

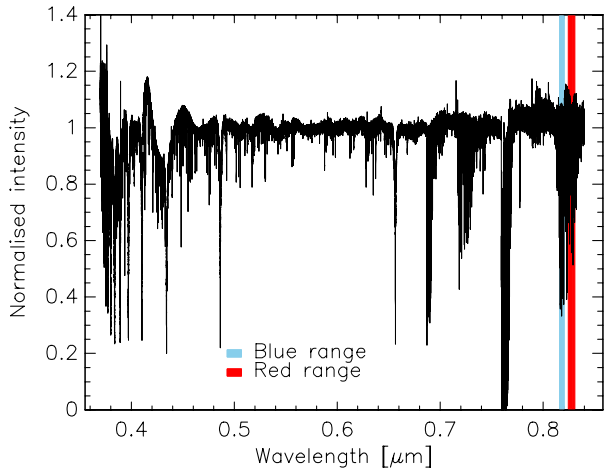

Fig. 2. Example of whole spectrum taken by BESO; the blue and red fitting region are shown in blue and red.

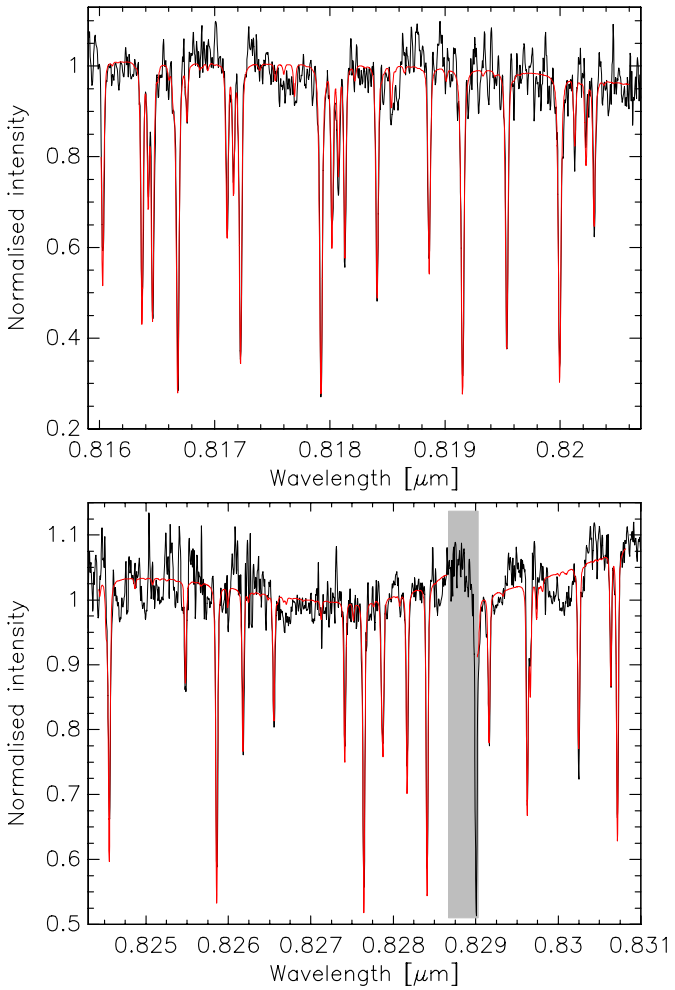

Fig. 3. *Top*: example of the fitting of the blue range. *Bottom*: an example of the fitting of the red range. The shaded region represents the zone that was excluded from the fit by the `molecfit` code.

the same results. The so-called blue range covered the wavelength from 816.01 to 820.60 nm, while the red range was defined from 824.43 to 828.67 and from 829.02 to 830.84 nm. In the red range we had to skip the region from 828.67 to 829.02 nm because of a strong instrumental artefact that most likely originates from an overlap of orders in the echelle spectrograph. The fitting of the sample spectrum for the two ranges is shown in Fig. 3. For a detailed description of the methods and how to use `molecfit`, see Smette et al. (2015).

During the manual investigation of a small subset of data that was undertaken to optimize the initial conditions for the automated fitting routine, some spectra failed to be fit automatically. This was due to poor background calibration, poor matching of orders of the echelle spectrograph, or some instrument and data reduction pipeline artefacts. Since a manual selection of the individual fits was not possible for the larger data sample, we used a test data set of three months to develop the selection criteria for the automatic rejection of spectra where the fits failed. In a trade-off between completeness and reliability, we decided for the conservative approach of higher reliability and thus probably missed some good data points. After the rejection, the PWV from the blue range was adopted for the final result (see below), while the red range was only used as a control set. We applied three criteria to select the results:

1. We selected five narrow windows in both ranges (with 108 and 106 spectral pixels each in total) on top of the strongest spectral features. They were selected to compare the obtained model and the data, without having to include a large amount of pixels where no absorption is applicable. The latter pixels were only used for `molecfit` to derive the stellar continuum. The model from fitting the whole range was compared with the data only in those windows, building a χ^2 value. We only used those PWV results where the degree of freedom of the fit (5 in our case) corresponds to a statistical confidence level of $\alpha = 0.05$.
2. We used the two-sample Kolmogorov-Smirnov test to check if the observed and fitted spectrum were identical. We adopted only those results with a confidence level of $\alpha = 0.05$. This test is known to be very stable for undefined non-normal distribution functions (Marsaglia et al. 2003).

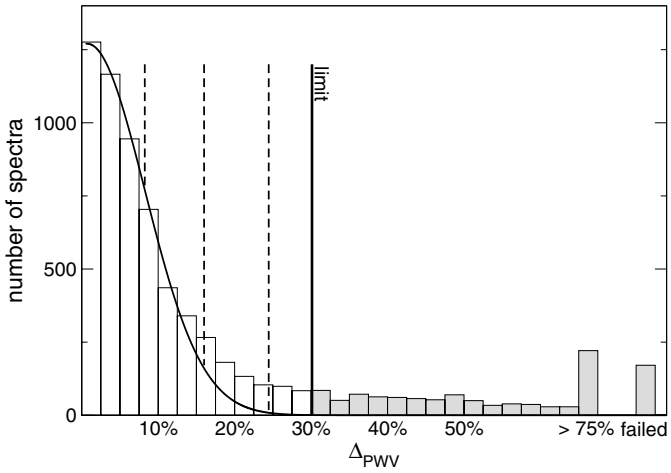

Fig. 4. Distribution of the differences Δ_{PWV} and the Gaussian distribution with a rms of 7.95% found up to the 2σ boundary. The dashed lines mark the 1, 2 and 3σ limits, respectively. The shaded part marks the spectra rejected by the sample selection. The fitting of both or one of the ranges sometimes completely failed to fit spectral lines.

3. Finally, the differences were calculated as

$$\Delta_{PWV} = \left|(PWV_{red} - PWV_{blue}) / (\tfrac{1}{2}(PWV_{red} + PWV_{blue}))\right|$$

and are shown in Fig. 4. The main distribution until the 2σ level represents a normal distribution with an rms of 7.95%. Thus, this value was adopted as the typical individual error of the measurements. At larger Δ_{PWV} systematic errors distort the distribution function. Only spectra for which the independently derived PWV values from the two ranges did not differ by more than 30% ($\equiv 3.8\sigma$) were selected for the sample.

After applying these three criteria, we obtained PWV estimates for the final sample based on 5879 spectra from 918 nights. The resulting PWV values are given in Table 1. This corresponds to about 63% of all archive files. As we still cover 92% out of all the 996 nights, no bias towards better PWV by the selection process has been introduced.

While at normal conditions the values from the two fitting regions are expected to coincide very well, in extreme conditions (extremely dry and thus weak absorption or extremely wet and thus saturation effects), the values could have larger differences. In the red fitting range molecular absorptions are weaker. This part of the spectrum is therefore more difficult to fit in case of dry conditions. In addition, instrumental defects, most likely remnants of fringing, causing periodic wave structures in the continuum of the star, are stronger in the red spectral range. Manual control samples also showed that these can be a source for some of the larger differences. After the selection mentioned above based on the control set and the statistical reliability, we adopted only the results from the blue range for the following analysis because the H_2O absorption is stronger there. Furthermore, the range covers a shorter wavelength region in total and thus is less affected from inter-order errors in the data reduction of the echelle spectrograph. It is assumed that the fits are more accurate there. Finally, for the spectra that were not rejected, only an extremely weak systematic effect between the results of the two ranges was found (Fig. 5).

3.2. Homogeneity of the sky

An important consideration for a site is the homogeneity of the sky. A large number of observations are required for such an analysis to obtain statistically strong results. In our case we were able to combine data from the full six-year period to separate seasonal and short-term variations from long timescale trends. We tested the spatial homogeneity of the PWV above the site by dividing the sky into 30° azimuth and 10° zenith distance bins, resulting in a polar coordinate grid of 9×12 fields. As `molecfit` recalculates the column density with respect to the zenith solution of the profile, the results are cleaned from effects that are due to the airmass. For each bin we calculated a 1.5σ clipped mean. The bins where the zenith distance is smaller than 60° have an average PWV of 3–4 mm, and the distribution is fairly homogeneous and independent of the direction (Fig. 6). In particular, no East-West asymmetry can be identified that would be due to the ~35 km distant Pacific coast and/or the air upstreaming the mountains. Bins with higher zenith distances (>60°) are statistically not reliable, as they contain only between one to ten measurements over the whole period of six years and were not used for analysis. The same is true for the two fields where the zenith distance is between 50° and 60° and the azimuth is between 0° and 60°, which have fewer than 25 measurements.

These findings are consistent with the results obtained by Querel & Kerber (2014) for Paranal. Using all-sky scans that were obtained every 6 h over a period of 21 months (down to 27.5° elevation), they reported that the PWV over Paranal is remarkably uniform with a median variation of 0.32 mm (peak to valley) or 0.07 mm (rms). The homogeneity is a function of the absolute PWV, but the relative variation is fairly constant at 10% (peak to valley) and 3% (rms). Variations like this will not have a significant impact on the analysis of astronomical data, and they concluded that observations are representative for the whole sky under most conditions.

3.3. Comparison and verification with Cerro Paranal

We compared BESO PWV results with those from Cerro Paranal (Kausch et al. 2015) to verify our results (see Fig. 7). Kausch et al. (2015) used X-Shooter data in the same way, by fitting the water vapour bands with `molecfit`. While the typical seasonal variations follow the same trends well at both sites, there is no clear signature of the moderate-to-strong El Niño (Ludescher et al. 2013) during the Chilean summer (December to March). Interestingly enough, Otárola et al. (2015) reported an unusually large number of extremely dry ($\leq$0.50 gr/m^3 H_2O) and very dry ($\leq$0.65 gr/m^3 H_2O) events for 2008–2010 by measuring the absolute humidity at 30 m height above Paranal. These events were two to three times more frequent than in other years. Thus, it seems that the 2009/2010 El Niño event did not cause more humid conditions at Cerro Paranal.

To obtain widely bias-free and comparable data sets, only those spectra of the X-Shooter and BESO samples were selected that were taken nearly simultaneously (within 1.5 h). This results in 3154 pairs of data. The resulting median distribution as function of the months for both sites is shown in Fig. 8, where the uncertainty varies between 4% and 16%. The difference of the two sites is especially obvious during the more humid summer months of December through February. For nights with coincident observations the median PWV for Cerro Murphy (BESO) is 2.43 mm, while it is 2.96 mm for Cerro Paranal (X-Shooter). This difference of 22% is significantly larger than expected from the difference of the altitude (2817

Table 1. PWV over Cerro Armazones derived from BESO data.

Index	Date yyyy-mm-dd	Time (UT) hh-mm-ss	PWV from BESO (mm)	PWV from GDAS (mm)	Azimuth (deg)	Altitude (deg)
1	2008-12-11	09-05-30	2.846	10.833	168.5387	53.6006
2	2008-12-11	09-16-43	2.613	10.851	170.8032	54.0580
3	2008-12-11	09-35-45	2.585	10.880	174.8069	54.6009
4	2008-12-11	10-03-10	2.729	10.915	180.7699	54.8423

Notes. Only a portion of this table is shown here. A full version is available at the CDS.

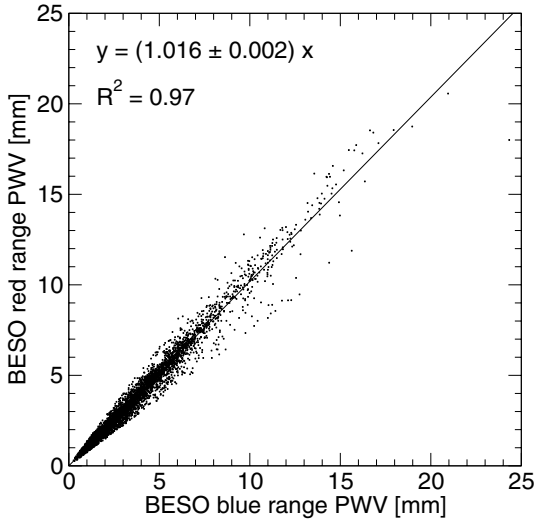

Fig. 5. Regression between the results of the red and the blue range fit for all spectra used in the final analysis.

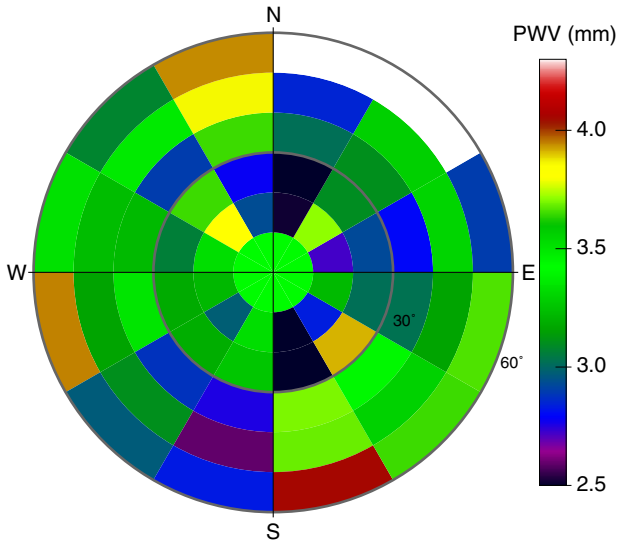

Fig. 6. 1.5σ truncated mean PWV for each field on the sky. Bins where the zenith angle exceeds 60 degrees contain no more than ten measurements and sometimes only a single one, while there are typically 100 to 200 measurements at all higher sky positions.

and 2635 m for Cerro Murphy and Cerro Paranal, respectively), using the scale-height of 1800 m found by balloon-born radiosondes from Antofagasta for altitudes above 2 km by Otárola et al. (2011). As these authors showed, the scale height in the Atacama desert can be lower under dry conditions. However, a randomly sampled spot check of the `molecfit` results from our sample with 20 probes around the median PWV revealed that

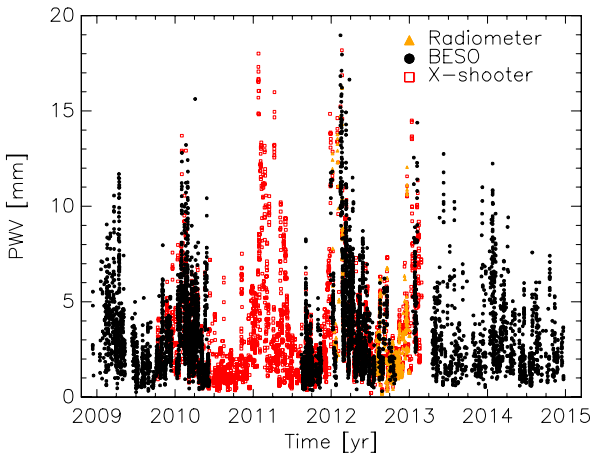

Fig. 7. Complete data sample from BESO measurements (this work) and the X-Shooter and LHATPRO radiometer data taken from the sample of Kausch et al. (2015).

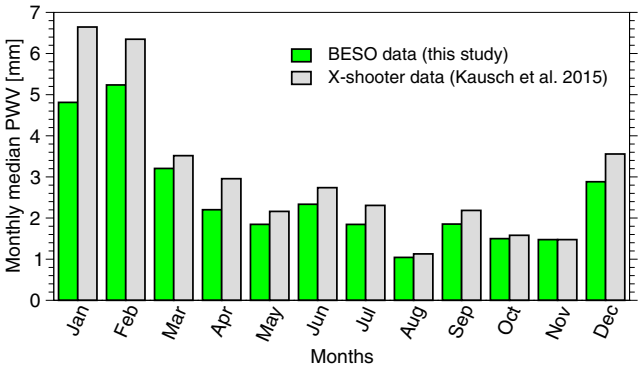

Fig. 8. Monthly median values of the PWV at Cerro Paranal and Cerro Murphy, using only those measurements where the observing times do not differ more than 1.5 h. The subsample sizes are 228, 434, 458, 330, 380, 96, 36, 232, 524, 212, 76, and 148, from January to December.

the scale-height agreed well at these average conditions. Using `molecfit`, including ground-based meteorological data (Smette et al. 2015), together with data from Cerro Paranal leads to a theoretical difference due to the altitude of only about 8%. The PWV as a function of site altitude given by Otárola et al. (2010) leads to 8.2%. This was obtained by comparing the five tested TMT candidate sites, which cover an altitude range of 2290 m to 4480 m.

To supplement this, we compared the BESO PWV with the values derived from GDAS and with those observed within 1.5 h with X-Shooter and with the verification data set of the LHATPRO radiometer (Kausch et al. 2014, 2015). In Fig. 9 we show the linear correlation ($y = Ax$) of the BESO data with those from Cerro Paranal. The resulting coefficients and

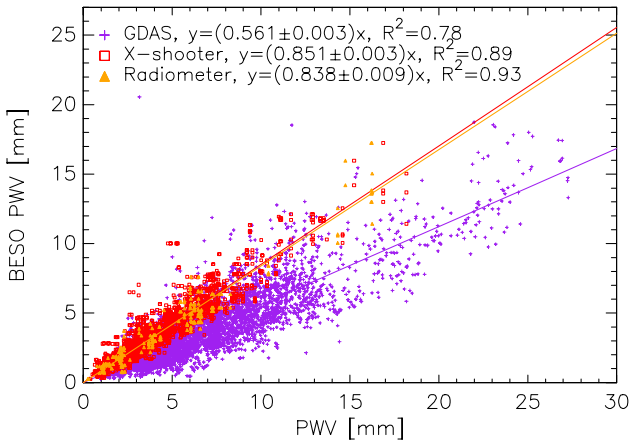

Fig. 9. Linear fits of X-Shooter, radiometer, and GDAS PWV at the abscissa vs. BESO PWV at the ordinate.

Table 2. Comparison of BESO PWV with those from Cerro Paranal and GDAS data for Cerro Murphy.

Data	A	R^2
X-Shooter	0.851 ± 0.003	0.89
Radiometer	0.838 ± 0.009	0.93
GDAS	0.561 ± 0.003	0.78

Notes. Linear fitting $y = A\,x$ was performed between pairs of PWV data.

R^2 values are given in Table 2. The BESO and X-Shooter data show a nearly identical slope (0.85) to that of BESO and the verification data set from the LHATPRO radiometer (0.84); with R^2 of 0.89 and 0.93, respectively. We therefore conclude that the LHATPRO radiometer verification can also be used for BESO.

The R^2 of BESO with GDAS data is 0.78 (Fig. 9). The GDAS data can be applied to predictions at locations far from the coast, on the other side of the Andes mountains, at the Auger observatory (Keilhauer 2015), but they clearly do not work in this zone of the Atacama desert. GDAS predictions systematically overestimate the PWV by 52%. Similar results were found for Cerro Paranal, but using locally improved GDAS profiles merged with ground-station meteorological data (Kausch et al. 2015).

4. Conclusions and outlook

4.1. PWV over Cerro Murphy

As already shown for Cerro Paranal in Kausch et al. (2015), spectral feature fitting by `molecfit` can successfully be used to investigate the PWV content in the Earth's atmosphere. The resulting PWV from Cerro Murphy, southwest of Cerro Armazones, are systematically lower than those from Cerro Paranal. The effect is stronger than expected from the altitude difference of 182 m, assuming the water vapour vertical distribution at the median conditions. The PWV is homogeneous and does not show any major sky direction asymmetries or trends within the six years of the study, although it covers the El Niño event 2009/10. Thus, it is possible to parameterize the sky only by means of zenith distance, without including azimuth dependencies. We showed that a very small telescope facility is able to provide an atmospheric monitoring capability with results fully comparable to those from the large telescopes. Moreover, it is clear that the interpolated data from GDAS are too inaccurate. Recently, two independent local refinement calculations of these coarse-grid weather models were presented by Lascaux et al. (2015) and Marín et al. (2015). Certainly, a comparison study of these methods with our results would be a further step. For this or other studies we offer to provide our resulting atmosphere profiles electronically.

4.2. Atmosphere studies at the CTA

Up to now, data reduction uses only simple integrated profiles throughout the whole atmosphere as a function of the airmass, or if very high accuracy is required, only uses nearby calibrators (e.g. differential photometry or iso-airmass telluric standards). The latter is not always possible or requires a large calibration plan. The first option suffers from missing information on the azimuth dependence, and is not sufficient to describe the light propagation of sources located in the atmosphere as is the case for γ-ray astronomy if using Čerenkov radiation.

When individual species that behave differently as a result of distributions other than the classical exponential scale height are used, real height profiles are especially important. The distribution of water vapour is strongly concentrated in the lower 10 km and thus does not follow the simple dependencies that are normally used for wide-band filter extinction curves.

Molecules in some distinct layers have to be treated specifically. An important example for this is ozone. Nearly the entire ozone absorption occurs in the stratosphere. It has to be removed from the extinction curve derived by photometry (Janeček et al. 2015; Ebr et al. 2015) for the CTA data reduction. To measure the variation of the tropospheric layers, our methods of ground-based spectroscopy presented here will be not sensitive enough. With the standard profiles of our sky model (Noll et al. 2012), we calculated the average fraction of the tropospheric ozone from the ground at 2 km to 10 km. As it only contributes about 6% to the total ozone absorption throughout the whole atmosphere, the error introduced by assuming a constant low fraction of tropospheric ozone on the total calculation is small. The strong contribution from the high atmosphere has to be derived separately from other sources of extinction and subtracted from the overall absorption. The Chappuis bands at $500 < \lambda < 700$ nm absorb and scatter significantly up to 4% at zenith. This is already essential, as the flux calibration specification for CTA is 5–7%. However, they only show very shallow and highly blended absorption structures. Our spectra do not cover the blue to ultraviolet light sufficiently well to also model the ozone variation in the Huggins bands ($\lambda < 400$ nm), which are stronger and show more characteristic features. These bands would be more appropriate for measuring the total ozone column. Therefore, a proposed CTA installation should be extended to the ultraviolet until 320 nm to fit the profile from the Huggins bands. The contribution of the Chappuis bands can then be calculated by our radiative transfer codes (Kimeswenger et al. 2015, Fig. 2).

Acknowledgements. We would like to thank the referee for the comments and very detailed suggestions. Furthermore, we thank Angel Otárola for providing us his full presentation of the EWASS15 conference. We thank Christian Westhues and Thomas Dembsky from Ruhr Universität Bochum for their help in accessing the BESO archive. M.L. was funded by the Comité Mixto ESO-Gobierno de Chile in the project Investigación Atmosférica con Instrumentación Astronómica. `Molecfit` was designed in the framework of the Austrian ESO In-Kind project funded by BM:wf under contracts BMWF-10.490/0009-II/10/2009 and BMWF-10.490/0008-II/3/2011. S.N and S.U. are funded by the Austrian Science Fund (FWF): P26130 and W.K. is supported by the project IS538003 (Hochschulraumstrukturmittel) provided by the Austrian Ministry for Research, Investigation and Economy (BM:wfw).

References

Chacón, A., Cuevas, O., Pozo, D., et al. 2011, in Rev. Mex. Astron. Astrofis. Conf. Ser., 41, 20

Clough, S. A., Shephard, M. W., Mlawer, E. J., et al. 2005, J. Quant. Spectr. Rad. Transf., 91, 233

Ebr, J., Janecek, P., Prouza, M., Blazek, J., & CTA Consortium 2015, 34th Int. Cosmic Ray Conf. (ICRC2015), The Hague, The Netherlands [arXiv:1508.06798]

Fuhrmann, K., Chini, R., Hoffmeister, V. H., et al. 2011, MNRAS, 411, 2311

Hodapp, K. W., Chini, R., Reipurth, B., et al. 2010, SPIE Conf. Ser., 7735, 77351A

Janeček, P., Prouza, M., & Ebr, J. 2015, EPJ Web Conf., 89, 3006

Kausch, W., Noll, S., Smette, A., et al. 2014, in EGU General Assembly Conference Abstracts, 16, 13979

Kausch, W., Noll, S., Smette, A., et al. 2015, A&A, 576, A78

Keilhauer, B. 2015, EPJ Web Conf., 89, 2001

Kerber, F., Querel, R., Hanuschik, R., et al. 2010, in SPIE Conf. Ser., 7733, 77331M

Kerber, F., Rose, T., Chacón, A., et al. 2012, in SPIE Conf. Ser., 8446, 84463N

Kerber, F., Querel, R. R., Rondanelli, R., et al. 2014, MNRAS, 439, 247

Kimeswenger, S., Kausch, W., Noll, S., & Jones, A. M. 2015, EPJ Web Conf., 89, 1001

Lascaux, F., Masciadri, E., & Fini, L. 2015, MNRAS, 449, 1664

Ludescher, J., Gozolchiani, A., Bogachev, M. I., et al. 2013, PNAS, 110, 11742

Mahoney, T., Muñoz-Tuñón, C., & Varela, A. M. 1998, New Astron. Rev., 42, 417

Marín, J. C., Pozo, D., & Curé, M. 2015, A&A, 573, A41

Marsaglia, G., Tsang, W. W., & Wang, J. 2003, J. Stat. Software, 8, 18

Noll, S., Kausch, W., Barden, M., et al. 2012, A&A, 543, A92

Otárola, A., Travouillon, T., Schöck, M., et al. 2010, PASP, 122, 470

Otárola, A. C., Querel, R., & Kerber, F. 2011, ArXiv e-prints [arXiv:1103.3025]

Otárola, A., Kerber, F., & Rondanelli, R. 2015, https://events.kuoni-dmc.com/ei9/images/EWASS15/Abstracts_2015/index.htm

Querel, R. R., & Kerber, F. 2014, in SPIE Conf. Ser., 9147, 92

Querel, R. R., Naylor, D. A., & Kerber, F. 2011, PASP, 123, 222

Rose, T., Crewell, S., Lohnert, U., & Simmer, C. 2005, Atm. Res., 75, 183

Rothman, L. S., Gordon, I. E., Barbe, A., et al. 2009, J. Quant. Spectr. Rad. Transf., 110, 533

Schöck, M., Els, S., Riddle, R., et al. 2009, PASP, 121, 384

Skidmore, W. & Travouillon, T. 2015, J. Phys. Conf. Ser., 595, 012033

Smette, A., Sana, H., Noll, S., et al. 2015, A&A, 576, A77

Steiner, I., Seifert, W., Stahl, O., et al. 2006, in SPIE Conf. Ser., 6269, 62692W

Steiner, I., Stahl, O., Seifert, W., Chini, R., & Quirrenbach, A. 2008, in SPIE Conf. Ser., 7014, 70144H

Varela, A. M., Vázquez Ramió, H., Vernin, J., et al. 2014, PASP, 126, 412

Vázquez Ramió, H., Vernin, J., Muñoz-Tuñón, C., et al. 2012, PASP, 124, 868

Vernin, J., Muñoz-Tuñón, C., Sarazin, M., et al. 2011, PASP, 123, 1334